Materials Today Bio 20 (2023) 100645

Contents lists available at ScienceDirect

Materials Today Bio

journal homepage: www.journals.elsevier.com/materials-today-bio

Carrier-free delivery of thymopentin-regulated injectable nanogels via an enhanced cancer immunity cycle against melanoma metastasis

Ning Ding [a,1], Kai He [a,1], Hailong Tian [b,1], Lei Li [a], Qiong Li [b], Shuaijun Lu [c], Ke Ding [d], Jiaqi Liu [e], Edouard C. Nice [f], Wei Zhang [b], Canhua Huang [a,b,*], Yong Tang [g,**], Zhisen Shen [h,***]

[a] School of Basic Medical Sciences, Chengdu University of Traditional Chinese Medicine, Chengdu, 611137, PR China
[b] Department of Biotherapy, Cancer Center and State Key Laboratory of Biotherapy, West China Hospital, Sichuan University, Chengdu, 610041, China
[c] Ningbo Hospital of Ningbo University 247 Renmin Road, Jiangbei District Ningbo, Zhejiang, 315020, China
[d] Clinical Genetics Laboratory, Affiliated Hospital, Chengdu University, Chengdu 610081, China
[e] International School of Public Health and Whole Health, Hainan Medical University, Haikou, 571199, PR China
[f] Department of Biochemistry and Molecular Biology, Monash University, Clayton, VIC, 3800, Australia
[g] Rehabilitation, Chengdu University of Traditional Chinese Medicine, Chengdu 610075, China
[h] Department of Otorhinolaryngology and Head and Neck Surgery, The Affiliated Lihuili Hospital, Ningbo University, 315040 Ningbo, Zhejiang, China

ARTICLE INFO

Keywords:
Thymopentin
Nanogel
Cancer immunity cycle
Immunogenic cell death
Chemo-immunotherapy
Melanoma metastasis

ABSTRACT

Thymopentin (TP5), a clinically used immunomodulatory pentapeptide, can efficiently promote thymocyte differentiation and influence mature T-cell function, thus playing an essential role in the cancer immunotherapy. However, the excellent water solubility and high IC50 of TP5 result in an uncontrolled release behavior, requiring a high loading efficiency to achieve high dosage. Here in, we reported that TP5, combined with specific chemotherapeutic agents, can co-assemble into nanogels due to multiple hydrogen bonding sites. The co-assembly of TP5 with chemotherapeutic agent doxorubicin (DOX) into a carrier-free and injectable chemo-immunotherapy nanogel can enhance the cancer immunity cycle against melanoma metastasis. In this study, the designed nanogel guarantees high drug loading of TP5 and DOX and ensures a site-specific and controlled release of TP5 and DOX with minimal side effects, thus addressing the bottlenecks encountered by current chemo-immunotherapy. Moreover, the released DOX can effectively induce tumor cell apoptosis and immunogenic cell death (ICD) to activate immune initiation. Meanwhile, TP5 can significantly promote the proliferation and differentiation of dendritic cells (DCs) and T lymphocytes to amplify the cancer immunity cycle. As a result, this nanogel shows excellent immunotherapeutic efficacy against melanoma metastasis, as well as an effective strategy for TP5 and DOX application.

1. Introduction

Melanoma is a malignant skin tumor which arises from the malignant transformation of melanocytes. Patients with advanced melanoma are prone to metastasis and have poor clinical prognosis [1,2]. Besides conventional cancer therapies including chemotherapy, immunotherapy is effective against various cancers, including melanoma [3]. With the development of nanotechnology, chemotherapy combined with immunotherapy serves as an effective strategy for the treatment of melanoma [4,5]. TP5 (Arg-Lys-Asp-Val-Tyr, RKDVY), an immunomodulatory pentapeptide with suitable biocompatibility and biodegradability, can modulate the cancer immunity cycle by promoting thymocyte differentiation and influencing mature T cells function [6]. However, its high-water solubility results in burst or uncontrolled release, while the high IC50 requires high TP5 loading levels to achieve high dosage. Therefore, it has been a huge challenge to develop a robust TP5 system for efficient immunotherapy.

Importantly, we have found that TP5, combined with specific chemotherapeutic agents, can co-assemble into nanogels due to multiple hydrogen bonding sites [7]. Nanogels are attractive carrier materials for

* Corresponding author.School of Basic Medical Sciences, Chengdu University of Traditional Chinese Medicine, Chengdu, 611137, PR China
** Corresponding author.
*** Corresponding author.
E-mail addresses: hcanhua@scu.edu.cn (C. Huang), tangyong@cdutcm.edu.cn (Y. Tang), szs7216@163.com (Z. Shen).
[1] These authors contributed equally to this work.

https://doi.org/10.1016/j.mtbio.2023.100645
Received 20 January 2023; Received in revised form 18 April 2023; Accepted 24 April 2023
Available online 25 April 2023

drug delivery systems because of their unique microstructure, and they can also act as a reservoir for the delivery of various therapeutic agents [8,9]. Moreover, anthracycline chemotherapeutic agents like doxorubicin (DOX) can produce an excess of reactive oxygen species (ROS) to induce tumor cell apoptosis [10]. This further leads to the release of damage-related molecular patterns (DMAPs), such as high mobility group protein 1 (HMGB1), adenosine triphosphate (ATP), and heat shock protein-70 (HSP-70), to trigger ICD [11]. ICD can then induce immune responses to promote the maturation of dendritic cells (DCs), activation of cytotoxic T cells (CTLs), and depletion of regulatory T cells (Tregs) for enhanced TP5-mediated cancer immunity cycle [12].

Inspired by this, we rationally designed an injectable nanogel (TP5@DOX nanogels, Scheme 1) with a TP5-based immunoregulator and DOX-based ICD inductor to enhance the cancer immunity cycle against melanoma. This carrier-free and injectable nanogel shows a high drug loading capability for TP5 and DOX, allowing the site-specific and sustained release of TP5 and DOX in the tumor microenvironment to reduce side effects, thus overcoming the limitations encountered by current chemo-immunotherapy. Notably, the released DOX can effectively induce tumor cell apoptosis to trigger ICD, further provoking the cancer immunity cycle. Additionally, TP5 can regulate the immunosuppressive tumor microenvironment to enhance antitumor immunity. Unsurprisingly, the obtained TP5@DOX hydrogels showed robust immunotherapeutic efficacy with minimal side effects in suppressing primary and abscopal tumors and eliminating lung metastases. Therefore, our TP5@DOX hydrogel provides a new therapeutic strategy for melanoma immunotherapy via a simple co-assembly approach.

2. Results and discussions

2.1. Characterization of the nanogel system

We used a simple co-assembly strategy to obtain carrier-free and injectable TP5@DOX nanogels. As shown in Fig. 1A, the mixed solution of TP5 and DOX became as a red transparent nanogel as shown by the vial inversion method. Then we have examined the rheological characterization of the TP5@DOX hydrogel. As shown in Fig. S1, the storage modulus (G′) was much higher than the loss modulus (G″) at a body temperature of 37 °C, which indicated the gel status of TP5@DOX. Subsequently, we verified that the obtained TP5@DOX nanogels showed good injectability, realizing an injectable nanogel platform that could be used for immunotherapy (Fig. 1B). Moreover, compared to the zeta potential of TP5 solution (−14.067 ± 1.756 mV), the zeta potential of TP5@DOX solution was +22.833 ± 0.252 mV, suggesting that the positively charged DOX had been successfully introduced into the nanogel (Fig. 1C), which was consistent with the previous analysis. Furthermore, as shown in transmission electron microscopy (TEM) images (Fig. 1D and E), after pH adjustment, the TP5 solution formed nanospheres with a particle size of a few tenths of a nanometer, and with the addition of DOX, the non-covalent bonding of TP5 and DOX produced nanofibers of micron length with a few uniformly sized nanospheres distributed on the surface. According to previous reports, the generation of nanofibers originated from the formation of hydrogen bonds, but both negatively charged ICG and TP5 failed to form nanogels, so it was speculated that the formation of nanogels was related to the charge interaction between TP5 and DOX [7]. This carrier-free nanogel formation was clearly different from others [13]. It has been reported that nanospheres or proteins can act as cross-linking agents to mediate the interaction between supramolecular nanofibers and stabilize the

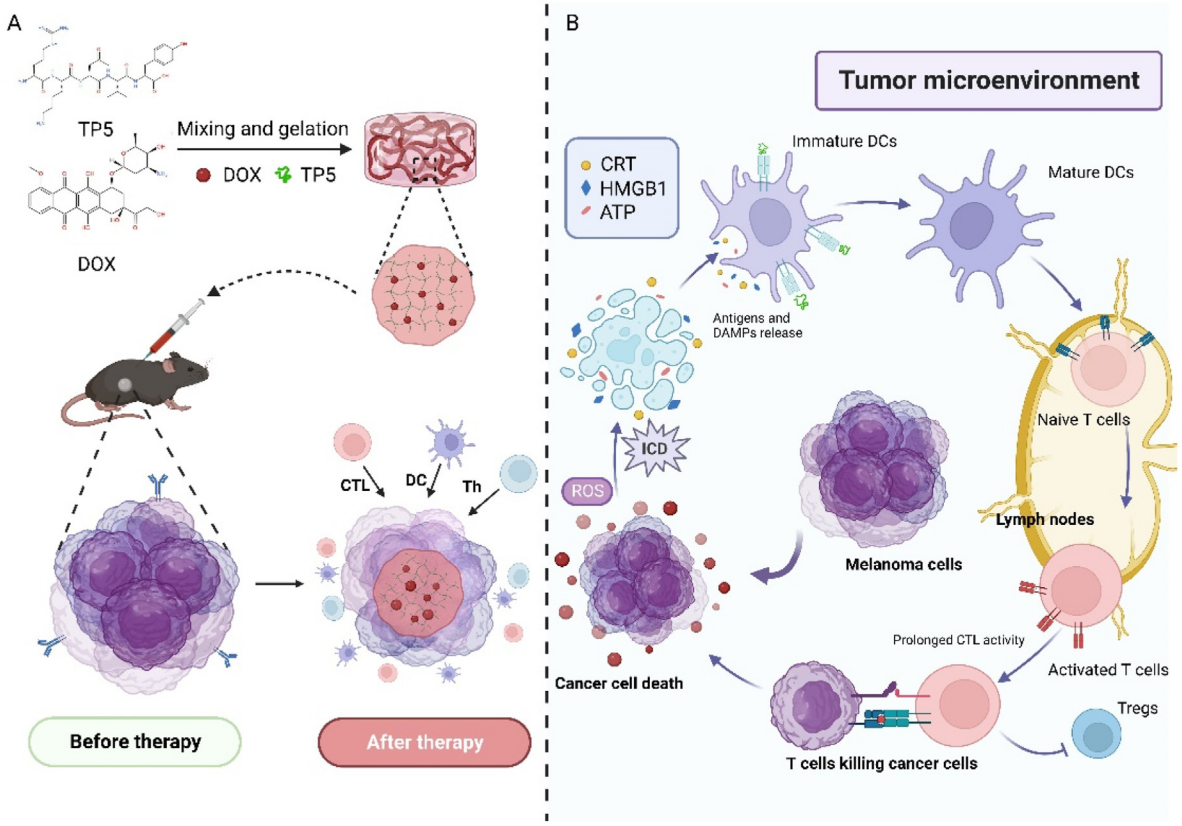

Scheme 1. Schematic diagram of the formation and application of carrier-free delivery of thymosin-modulated injectable nanogels. A) Co-assembly of TP5 and DOX to form nanogels for melanoma treatment. B) TP5@DOX nanogels enhance the cancer immune cycle against melanoma growth and metastasis.

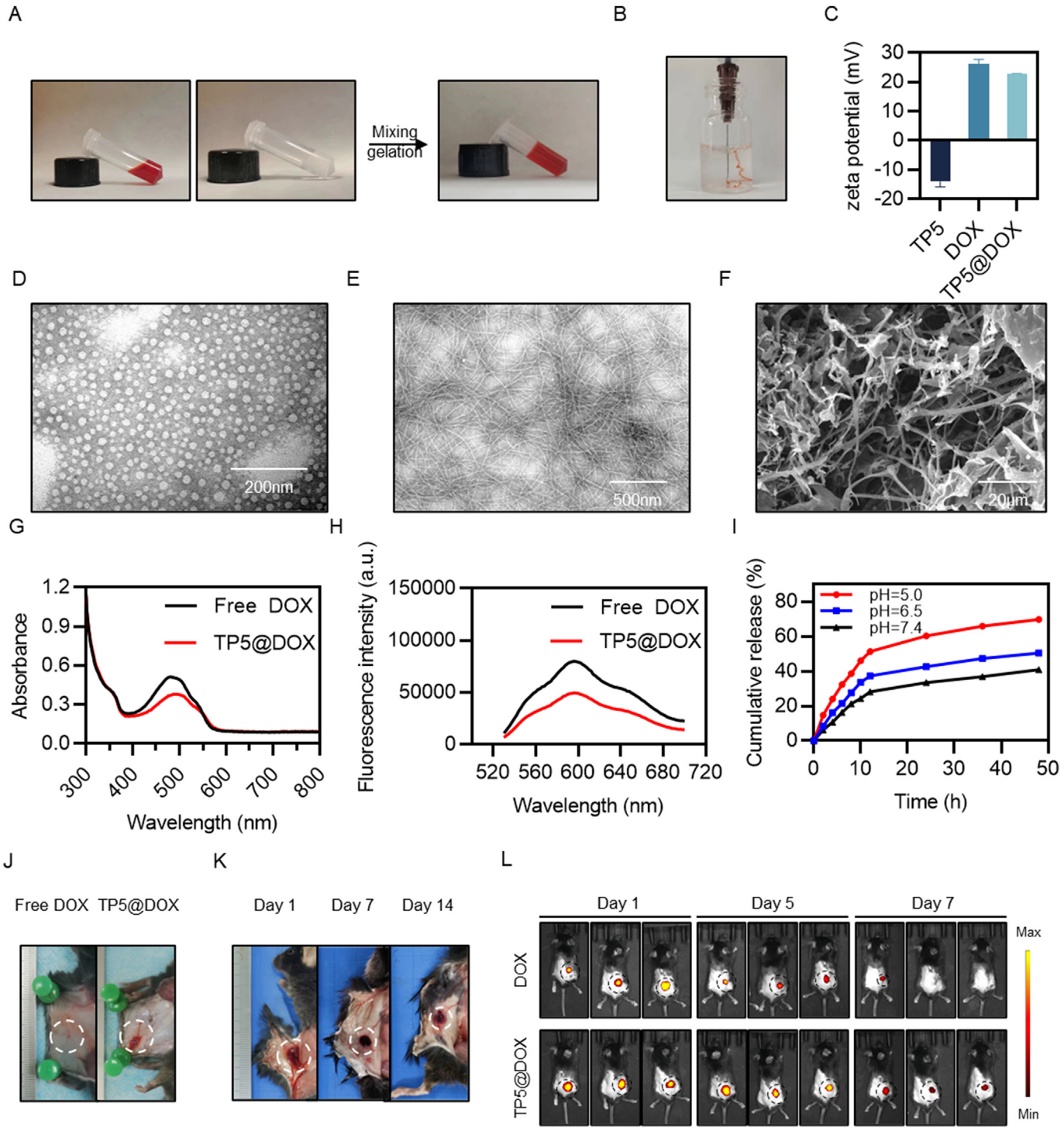

Fig. 1. Characterization of TP5@DOX nanogel. A) Photograph of TP5@DOX nanogel. B) Photograph showing injection of a TP5@DOX nanogel solution into PBS. C) Zeta potentials of TP5, free DOX, and TP5@DOX solutions. D) TEM image of TP5 solution. E) TEM image of TP5@DOX nanogel. F) SEM image of TP5@DOX nanogel after lyophilization. G) UV–Vis absorption spectra and H) fluorescence emission spectra of free DOX and TP5@DOX nanogels with identical DOX concentrations of 0.01 mg mL-1. I) Release behavior of DOX from TP5@DOX nanogels in media with different pH values (n = 3). Data are expressed as the mean ± SD. J) Photographs of TP5@DOX nanogel gelation behavior *in vivo*. K) Photographs of TP5@DOX nanogels degradation at specific time intervals *in vivo*. L) Fluorescent images showing the degradation behavior of TP5@DOX nanogel in tumor sites (n = 3).

structure of nanogels [14,15]. Scanning electron microscopy (SEM) was used to further describe the TP5@DOX nanogel morphology following lyophilization. As shown in Fig. 1F, the nanogel exhibited a typical structure of porous and loose interconnected fibers, but the surface of the fibers was not smooth, probably related to the presence of nanospheres. In addition, the free DOX and TP5@DOX nanogels had similar characteristic peaks as shown by their ultraviolet (UV) absorption and fluorescence spectra (Fig. 1G and H), and had similar fluorescence characteristics to those published previously for free DOX [16].

We also investigated the release behavior of DOX and TP5 from TP5@DOX nanogels *in vitro* in solution media with different pH values. Compared to the pH 7.4 solutions, pH 5.0 solutions have been frequently

used to mimic the acidic microenvironments in tumor sites [17]. We observed DOX and TP5 was released more rapidly and sustainably at pH 5.0 than at pH 7.4 (Fig. 1I and S2), suggesting that TP5@DOX nanogels could be suitable for antitumor therapy. Moreover, we examined the *in vivo* gelation and degradation of TP5@DOX nanogels by subcutaneous injection of TP5@DOX nanogels into the backs of C57BL/6 mice. As shown in Fig. 1J, the free DOX dispersed rapidly *in vivo*. In contrast, the TP5@DOX nanogel was able to quickly gelatinize and form a red gel that was not easily dispersed. Its presence under the skin underwent slow degradation and persisted for up to two weeks, indicating that it has long-term hydrodynamic stability (Fig. 1 K). Since DOX possesses red fluorescent properties, fluorescent signals by IVIS were used to verify the drug release from TP5@DOX nanogels *in vivo*. As shown in Fig. 1 L, fluorescent images showed that the TP5@DOX nanogel almost totally disrupted after a week, indicating that it had good hydrodynamic stability and could gradually release TP5 and DOX to enhance the cancer immunity cycle. Collectively, this indicates that the TP5@DOX nanogel was an excellent nanogel platform with sustainable release properties for long term treatment.

2.2. TP5@DOX nanogels inhibit the proliferation of melanoma cells in vitro

Effective cellular uptake of drugs is critical for antitumor effects [18]. To evaluate the cellular uptake effect of the TP5@DOX nanogel, two melanoma cell lines (human A375 and murine B16F10 cells) were selected. As seen in the fluorescent images (Fig. 2A), the TP5@DOX nanogel continued to accumulate intracellularly over time similar to DOX, which was a prerequisite for subsequent cytotoxicity evaluation. The cytotoxic effect of the TP5@DOX nanogel was assessed using MTT assays *in vitro*. The viabilities of both A375 and B16F10 cells gradually decreased with increasing TP5@DOX nanogel concentration (Fig. 2B), which was mainly dependent on DOX present in the TP5@DOX nanogel. As shown in Fig. S3, TP5 had insignificant killing effects on A375 and B16F10, while DOX had significant inhibitory effects on cell viability in a concentration-dependent manner. Subsequently, we only labeled the surviving tumor cells (A375 and B16F10 cells) with Calcein-AM after different treatments and evaluated the antitumor effect by the number of living cells. As shown in Fig. 2C, the number of green fluorescence was significantly reduced after doxorubicin administration, demonstrating its good antitumor effect. Furthermore, EdU assay results demonstrated that different treatments exhibited varying effects on the proliferation of melanoma cells, particularly showing inhibition with the TP5@DOX nanogel (Fig. 2D and E). Additionally, as shown in Fig. 2F, the results of the LDH assay indicated that the TP5@DOX nanogel was able to significantly disrupt the cell membrane integrity and stimulate the cells to release more lactate dehydrogenase, exhibiting strong cytotoxicity. In summary, the results showed that the TP5@DOX nanogel had good cytotoxicity *in vitro* and effectively inhibited melanoma cell proliferation.

2.3. The TP5@DOX nanogel trigger ICD in vitro

It has been shown that DOX induces not only apoptosis but also ICD in dying tumor cells through the production of excess ROS [10]. ICD is a specific form of cell death that triggers antitumor immune responses. The immune effects of ICD depend on the release of damage-associated molecular patterns (DAMPs), which include exposure of calmodulin (CRT) on the cell membrane and the release of high-mobility histone B1 (HMGB1) and the secretion of ATP [11]. Secreted DAMPs, induced dendritic cells (DCs) maturation and T cells activation, elicited a powerful anti-cancer immune response [19]. The 20,70-dichlorofluorescein diacetate (DCFH-DA) probe was used to evaluate whether DOX could overproduce ROS to initiate apoptosis in B16F10 cells. The results showed that the fluorescence intensity of the TP5@DOX nanogel was significantly stronger than that of PBS, TP5, and free DOX (Fig. 3A). These results were further validated by a flow cytometry assay (Fig. 3B).

Subsequently, we analyzed critical ICD biomarkers to show whether TP5@DOX nanogels might trigger ICD in melanoma cells. Calreticulin (CRT) can deliver an "eat-me" signal that ultimately leads to immunogenicity when exposed on the cell membrane during ICD [20]. As shown in Fig. 3C, immunofluorescence images demonstrated that the TP5@DOX nanogel could significantly increase CRT exposure to the cell membrane. Additionally, the increased fluorescence intensity detected by flow cytometry also indicated an increase in CRT proteins (Fig. 3D). Moreover, HMGB1 can also lead to transport from the nucleus to the cytoplasm and extracellular space in the process of ICD [21]. As shown in Fig. 3E, after treatment with the TP5@DOX nanogel the fluorescence in the nucleus was diminished and HMGB1 flowed into the cytoplasm. It has been shown that ATP is not only an important source of energy for tumor metastasis, but extracellularly released ATP also acts as a "find me" signal that mediates pro-inflammatory effects [22,23]. The concentration of ATP in intracellular and cell culture medium was examined after different treatments. As shown in Fig. 3F, the TP5@DOX nanogel group reduced the production of ATP in intracellular and increased its release to the extracellular region. In order to evaluate the immunological effect of TP5@DOX nanogel, its immune cytotoxicity was assessed by CCK8 assay, and the results are shown in Fig. S4. Moreover, as shown in Fig. S5, ELISA was used to detect pro-inflammatory cytokines (IL-2, IL-6, IL-10, TNF-α) in the supernatant of tumor cells treated with different formulations. Additionally, we used an *in vitro* co-culture assay to evaluate the effects of the TP5@DOX nanogel on the immunological cells *in vitro*. As shown in Fig. 3G and H, DOX@TP5 nanogels could significantly increase the proportion of DCs and $CD8^+$ T cells. These results strongly supported the potential of TP5@DOX nanogel to effectively trigger ICD to enhance antitumor immunity.

2.4. TP5@DOX nanogels inhibit bilateral tumor growth

During the ICD process, cells activate antitumor immune responses [12]. To support the immunoregulatory effects of TP5 for clinical use, we confirmed the antitumor immunological effect of the TP5@DOX nanogel to prevent melanoma metastasis *in vivo*. A bilateral subcutaneous B16F10 model using C57BL/6 mice was constructed (Fig. 4A). The tumors on the right and left sides were defined as primary and abscopal tumors, respectively [24]. As shown in Fig. 4B, we have used bioimaging experiments to further monitor the tumor growth in mice. The fluorescence intensity of the tumor in mice treated with the TP5@DOX nanogel was significantly reduced, supporting that this nanogel had excellent antitumor effects. Caliper measurements were used to monitor the growth of primary and abscopal tumors over a 2 week period (Fig. 4C). The fluorescence intensity of the tumor in mice treated with the TP5@DOX nanogel was significantly reduced, supporting that this nanogel had excellent antitumor effects. As shown in Fig. 4D, primary tumor growth was significantly inhibited in the TP5@DOX nanogel-treated group compared with the other groups. The free DOX-treated group had only a limited antitumor effect on primary tumor growth. Tumor suppression in the TP5-treated group was not obvious, probably because TP5 is an immunomodulator and did not cause ICD, therefore preventing it from exerting immunotherapeutic effects. For the abscopal tumors, tumor growth was distinctly delayed after treatment with TP5@DOX nanogel, revealing an inhibitory impact (Fig. 4B and D) that was superior to chemotherapy and immunotherapy alone [25]. On day 14 following injection, tumor tissues were collected for photography and weighing, and the tumor inhibition ratio was calculated. (Fig. 4E and F). As seen in Fig. 4G, the hematoxylin and eosin (H&E) staining images and histochemical KI67 staining images further verified that TP5@DOX nanogel could suppress tumor proliferation and cause tumor tissue injury. Additionally, the TUNEL assay confirmed that the TP5@DOX nanogel could induce tumor cell apoptosis.

Throughout the experiment, we observed that the body weight of the mice remained stable with no obvious changes across the different groups (Fig. S6). To further assess the safety of the nanogel for potential

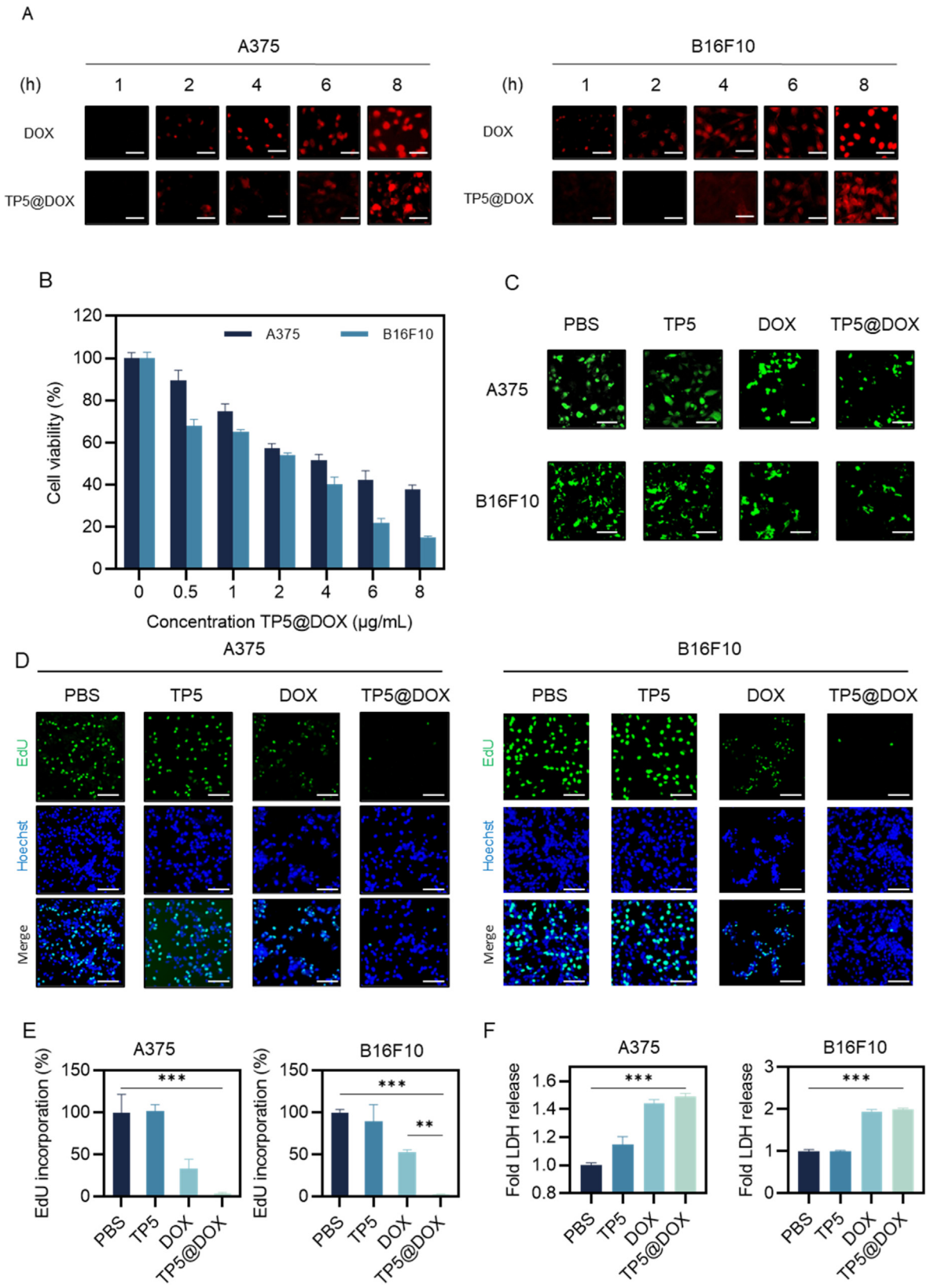

Fig. 2. TP5@DOX nanogels inhibit the proliferation of melanoma cells *in vitro*. A) Cellular uptake of free DOX and the TP5@DOX nanogel by A375 and B16F19 cells at different time points (scale bar = 50 μm). B) The cell viability of A375 and B16F10 cells after treatment with TP5@DOX by MTT assay (n = 3). C) CLSM images of A375 and B16F10 cells stained with Calcein-AM dye after incubated with different treatments. D) Fluorescence images of EdU detection in A375 and B16F10 cells (scale bar = 100 μm). E) Statistical analysis of the EdU incorporation rate of A375 and B16F10 cells. F) Analysis of LDH release in the supernatants of A375 and B16F10 cells incubated with different treatments for 24 h.

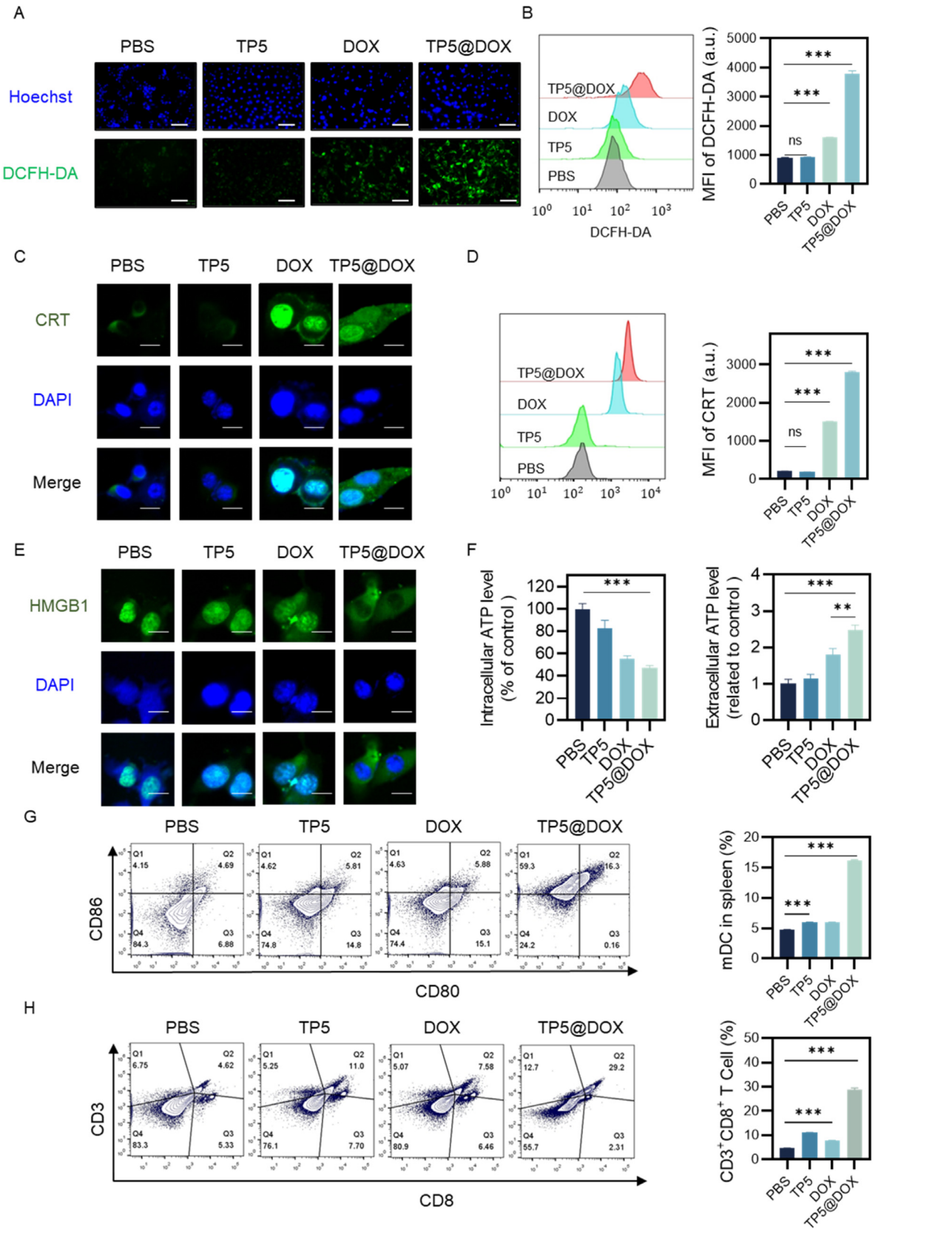

Fig. 3. TP5@DOX nanogel triggers ICD *in vitro*. A) Fluorescence images and B) flow cytometry analysis of ROS in B16F10 cells after different treatments (scale bar = 100 μm). C) CLSM images of CRT and E) HMGB1 in B16F10 cells after different treatments (scale bar = 20 μm). D) Flow cytometry analysis of the fluorescence intensity of CRT proteins in B16F10 cells after different treatments. F) Results of intracellular and extracellular ATP content measurement (n = 3). G) Flow analysis and quantitative analysis of DCs maturation after different treatments (n = 3). H) Flow analysis and quantitative analysis of $CD8^+$ T cells after different treatments (n = 3).

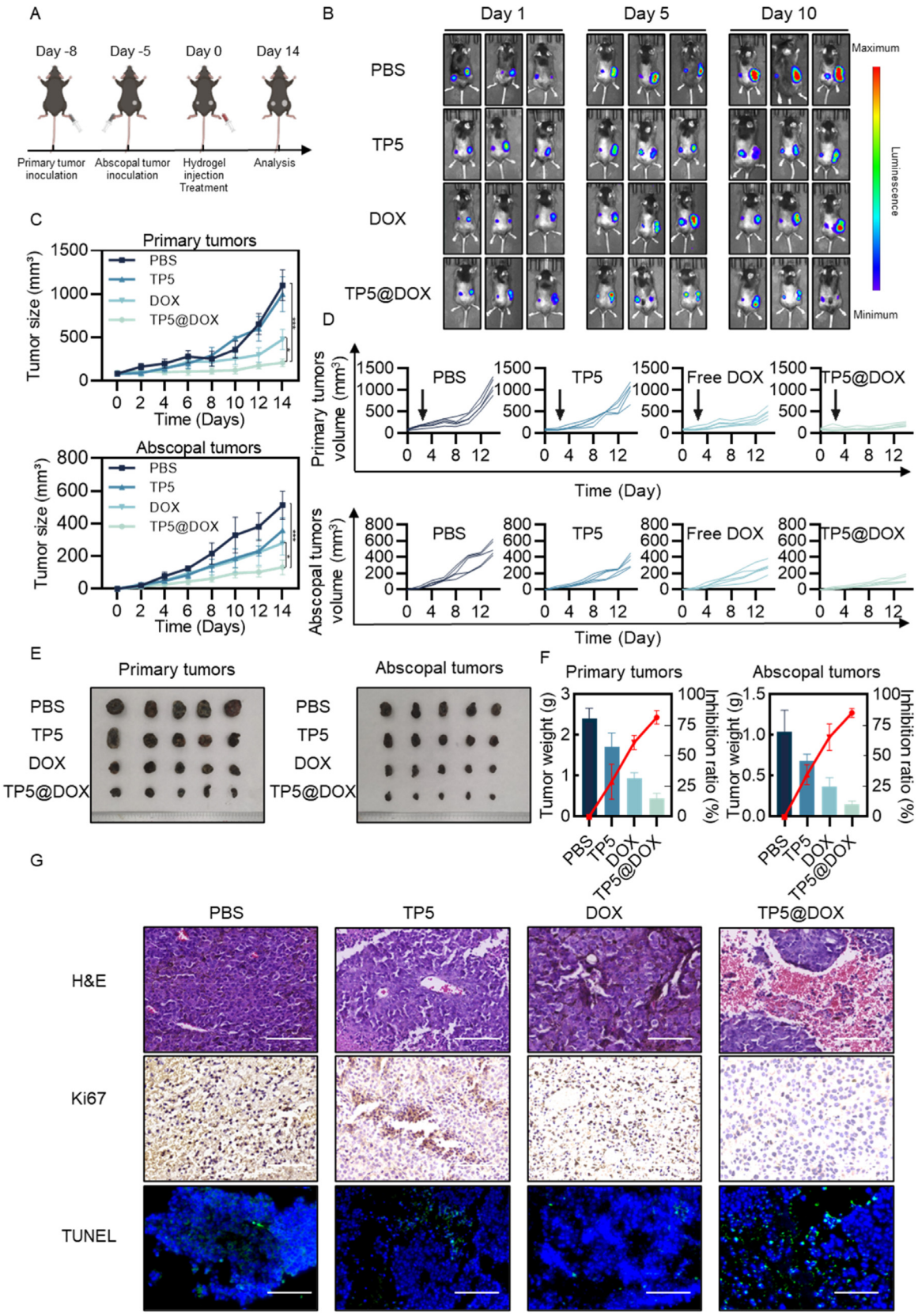

Fig. 4. TP5@DOX nanogel inhibits bilateral tumor growth *in vivo*. A) Schematic diagram of the construction and treatment of a bilateral tumor model in mice. B) Bioluminescence imaging of tumor growth of mice *in vivo*. C) The average tumor growth curves for primary and abscopal tumors. D) Individual tumor growth kinetics in mice subjected to different treatments. E) Representative images of primary and abscopal tumors 2 weeks after different treatments and F) tumor weights and tumor inhibition ratios of primary and abscopal tumors (n = 5). G) H&E staining images, histochemical Ki67 images and TUNEL fluorescence images of primary tumors extracted from mice after different treatments (scale bar = 100 μm).

translational therapy, we carried out biosafety-related pathological and toxicological serological analyses. As shown in Fig. S7, no significant histological damage was found in the main organs, such as the liver, heart, spleen, lung, and kidney as indicated by H&E staining. As shown in Fig. S8, the hepatorenal function of mice in the TP5@DOX nanogel-treated group remained in the normal range [26,27]. Interestingly, a significant increase in CK-MB was observed in the free DOX-treated group, while the level was lower in the TP5@DOX nanogel-treated group, indicating that the TP5@DOX nanogel effectively attenuated the cardiotoxicity of DOX with insignificant side effects [28]. This confirmed the excellent safety profile of the controlled release TP5@DOX nanogels.

2.5. The TP5@DOX nanogel induces antitumor immunological responses in vivo

To elucidate the potential mechanism of antitumor immunity of the TP5@DOX nanogel, the ratio of multiple immune cells *in vivo* was analyzed by flow cytometry after treatment. As shown in Fig. 5A, the proportion of mature DCs in lymph nodes (LNs) was significantly increased in the TP5@DOX nanogel-treated group due to the release of large amounts of tumor antigens from dying tumor cells, which can promote the transition of immature DCs into mature DCs [29]. Mature DCs, as the strongest antigen-presenting cells (APCs), bind to T-cell antigen receptors (TCRs) by presenting antigens and activating CTLs, and activated CTLs can effectively remove tumor cells and play an important antitumor immune role [30,31]. As shown in Fig. 5B, mice treated with the TP5@DOX nanogel had a significantly increased percentage of CTLs by flow cytometry analysis, which was 7.48 ± 0.56% in the spleen and 2.6 times higher than that in the PBS-treated group. As shown in Fig. 5C and D, the results of flow cytometry analysis of primary and abscopal tumors were similar, with an increased percentage of CTLs in tumors, indicating that the TP5@DOX nanogel could exert antitumor immune effects. Immunofluorescence images of $CD8^+$ T cells in primary and abscopal tumors have been supplemented with the DOX and TP5 group in Fig. 5E. This nanogel exhibited a greater population of $CD8^+$ T cell infiltrates in the primary and distant tumors compared with the DOX and TP5 group, which agreed with the previous results.

Helper T lymphocytes (Th), $CD4^+$ T cells, not only activate CTLs but also kill tumor cells by secreting cytokines and are important components of the immune system [32,33]. Naive CD4 T cells can differentiate into multiple subtypes, with Tregs being recognised as representative immunosuppressive cells. Treg cells inhibit the maturation of DCs and suppress the proliferation and differentiation of $CD8^+$ T cells in the tumor microenvironment [34,35]. Compared to the other groups, TP5@DOX nanogels effectively reduced the proportion of Treg cells in the spleen of mice, as shown by flow cytometry analysis (Fig. 5F). As shown in Fig. S9, we examined CD8 and FOXP3 in tumor tissues by Immunohistochemical analysis. TP5@DOX nanogel exhibited a greater population of $CD8^+$ T cell infiltrates in the primary and distant tumors compared with other treatments, which agreed with the immunofluorescence results and showed great potential for eliminating bilateral tumors by effective infiltration of activated T cells. Meanwhile, the TP5@DOX treatment also decreased the proportions of Tregs (Fig. S10). These results demonstrate that the TP5@DOX nanogel not only induces immune responses in the primary tumors but also regulates systemic immunological responses and exerts immunotherapeutic effects to inhibit the development of abscopal tumors.

2.6. TP5@DOX nanogel eliminates melanoma metastasis in vitro and in vivo

Melanoma is a highly metastatic skin malignancy [2]. However, scratch and migration experiments indicated that the TP5@DOX nanogel had the potential to inhibit B16F10 cells from metastasizing (Fig. 6A and B). Since the TP5@DOX nanogel induced efficient systemic antitumor immunological responses, we expected that the TP5@DOX nanogel could effectively prevent tumor metastasis. A melanoma lung metastasis model was developed (Fig. 6C) and used to investigate whether various treatments were effective in inhibiting tumor metastasis in the lung. After 3 weeks of local injection, mouse lung tissues were collected for photography and the number of nodules counted. In the TP5@DOX nanogel-treated group, the number of tumor metastases in lung tissues was markedly lower than that in the PBS-treated group, and the tendency of tumors to metastasis to the lungs was effectively suppressed. In contrast, the suppression effect was less obvious in the free DOX-treated group and minimal in the TP5-treated group (Fig. 6D and E). As shown in Fig. 6F, in the PBS-treated group, tumor metastasis was clearly observable and largest in the H&E-stained images of lung tissues, while in the TP5-treated group and DOX-treated group, the area of tumor metastasis was relatively reduced, while lung metastasis was insignificant in the TP5@DOX nanogel-treated group, providing additional evidence that TP5@DOX nanogels stimulate an effective systemic immune response and prevent tumor metastasis.

3. Conclusions

In summary, we designed an immunomodulatory peptide-based carrier-free and injectable nanogel containing chemotherapeutic agents and clinically approved molecular drugs (TP5 and DOX) for localized melanoma therapy. This carrier-free and injectable nanogel shows a high drug loading capability for TP5 and DOX, and results in site-specific and sustained release of TP5 and DOX in the tumor microenvironment to reduce side, thus overcoming the limitations encountered by current chemo-immunotherapy. Moreover, the TP5@DOX nanogel could remodel the immunosuppressive microenvironment and promote the proliferation and differentiation of antitumor immune cells to trigger a robust systemic immune response. Importantly, this TP5@DOX nanogel exerted a powerful suppressive effect on the growth and metastasis of melanoma. This novel carrier-free and injectable nanogel shows great potential for immunomodulatory therapy in melanoma, and provides a promising strategy for the clinical application of TP5 and DOX.

4. Materials and methods

4.1. Materials

Thymopentin (TP5) was purchased from Meilunbio. Doxorubicin hydrochloride (DOX) was obtained from Aladdin. Fetal bovine serum albumin (FBS) was purchased from Biowest. Dulbecco's modified Eagle's medium (DMEM) was purchased from Gibco. All assay kits, if not specified, were acquired from Beyotime. The antibodies used were as follows: anti-calreticulin, HMGB1, and CD8 were purchased from Santa Cruz Biotechnology; Ki67 was purchased from Bioss; anti-mouse antibodies (FITC-labeled CD3, FITC-labeled CD11c, FITC-labeled CD25, PE-labeled CD8a, PE-labeled CD86, APC-labeled CD4, APC-labeled CD80, Alexa Flour 647-labeled Foxp3) were all purchased from BioLegend. D-Luciferin, Potassium Salt was purchased from Yeasen.

4.2. Cell culture

Murine melanoma cells (B16F10), human melanoma cells (A375) and luciferase tagged murine melanoma cells (luc-B16F10) were cultured in DMEM separately containing 10% FBS and 1% antibiotics (100 U • mL^{-1} penicillin and 0.1 mg•mL^{-1} streptomycin, Beyotime) in an incubator containing 5% CO_2, at 37 °C.

4.3. Preparation and characterization of TP5@DOX nanogel

TP5@DOX nanogels were prepared by the following steps. First, the 16 mg of TP5 was dissolved with 470 μL of pure water and allowed to stand for 4 h at 4 °C, then added with 500 μL of DOX aqueous solution (2 mg mL^{-1}) and 30 μL of 0.1 M NaOH. The pH of the solution after the

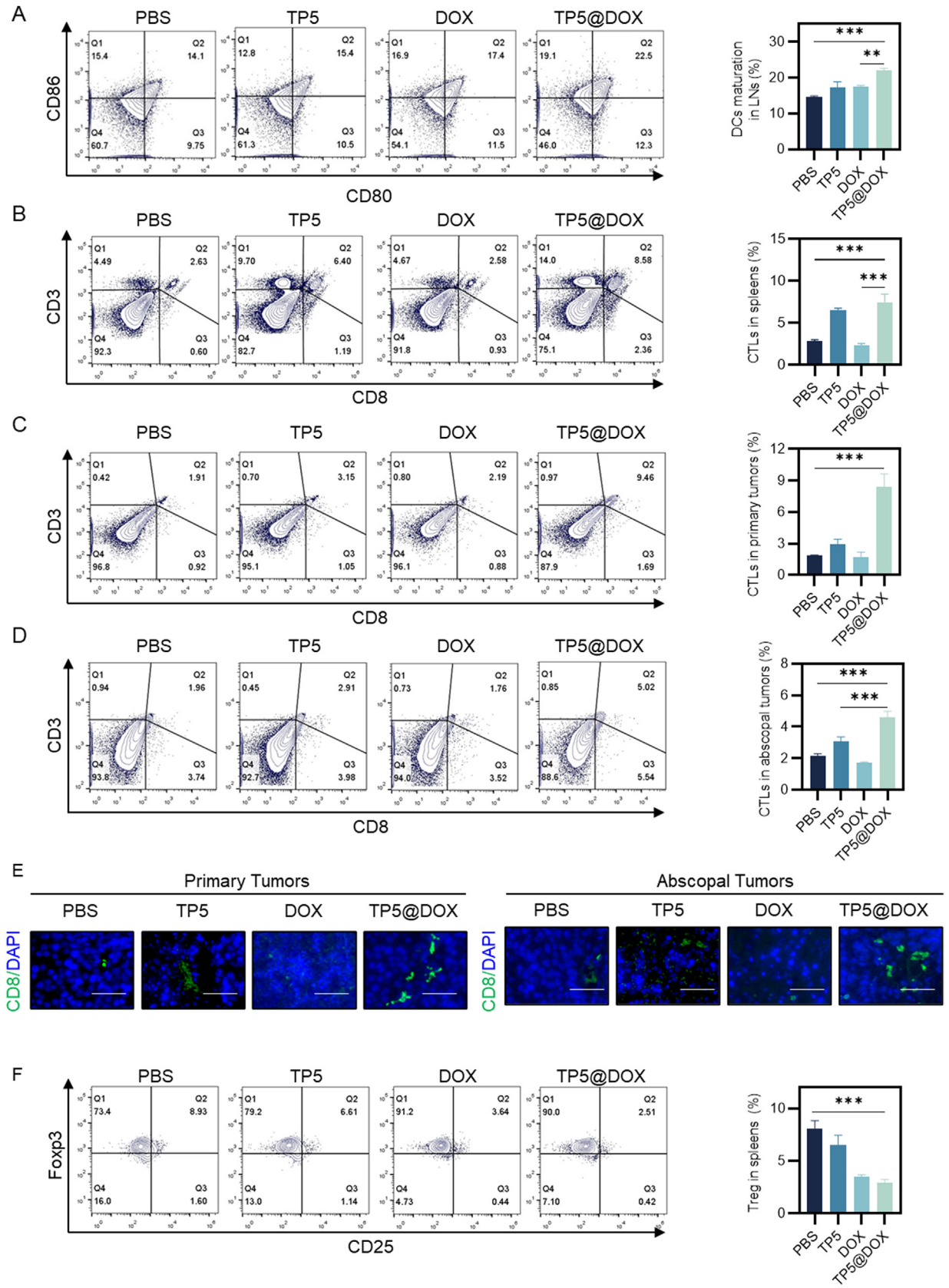

Fig. 5. The TP5@DOX nanogel induces antitumor immunological responses *in vivo*. A) Flow cytometry analysis and quantitative analysis of the percentage of mature DCs in LNs (n = 3). B) Flow cytometry analysis and quantitative analysis of the percent of CTLs in spleens (n = 3). C) Flow cytometry analysis and quantitative analysis of the percent of CTLs in primary tumors (n = 3). D) Flow cytometry analysis and quantitative analysis of the percent of CTLs in abscopal tumors (n = 3). E) Images of $CD8^+$ T cell-immunofluorescence staining of tumor tissues from mice after different treatments. Scale bar = 100 μm. F) Flow cytometry analysis and quantitative analysis of the percent of Tregs in spleens (n = 3).

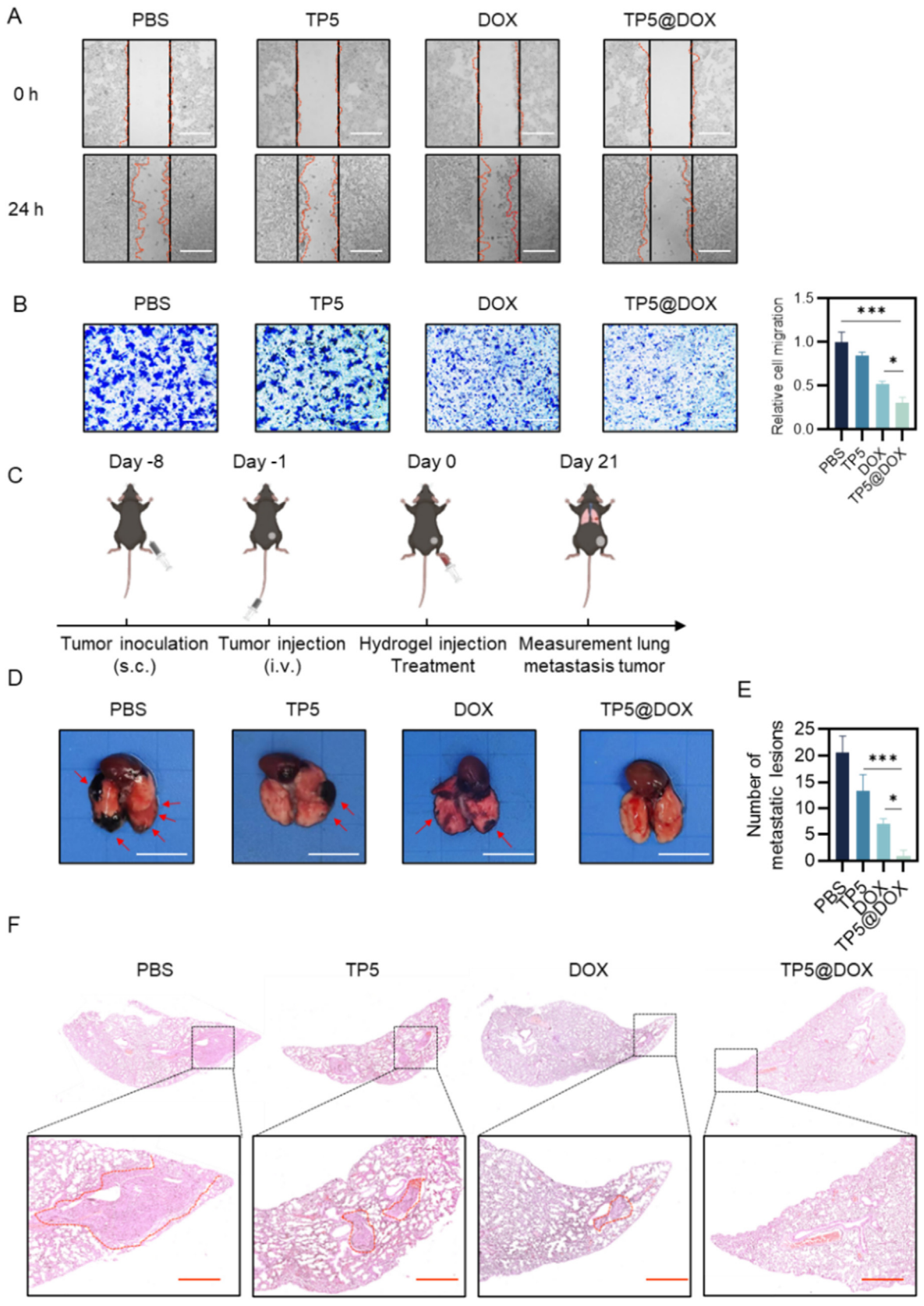

Fig. 6. TP5@DOX nanogel eliminates melanoma metastasis *in vitro* and *in vivo*. A) Light microscopy images of scratch wound assays of B16F10 cells at 0 h and 24 h after different treatments (scale bar = 100 μm). B) Light microscopy images (left) and analysis of the migration rate (right) of B16F10 cells at 24 h after different treatments (scale bar = 100 μm). C) Schematic diagram of the construction and treatment of a tumor metastasis model in mice. D) Representative images of pulmonary metastases from melanoma at week 3 after different treatments (scale bar = 1 cm) and E) statistics of the number of pulmonary metastatic lesions (n = 3). F) H&E staining images of lungs removed from mice after different treatments (scale bar = 500 μm).

above mixing was ~7, and the nanogel was formed after standing overnight at 4 °C. The morphology of the TP5@DOX nanogel was characterized by TEM, and the lyophilized powder obtained was characterized by SEM. After the nanogel was swelled, its UV–vis and fluorescence wavelength were measured by a Tecan Spark multimode microplate reader [36].

4.4. In vitro drug release behaviors from TP5@DOX nanogel

300 μL TP5@DOX nanogel was incubated with PBS at different pH values (pH 5.0, pH 6.5 and pH 7.4) at 37 °C with gentle shaking. The DOX and TP5 released within the designated time were characterized by an UV–vis spectrophotometer. The drug release rate was calculated from the standard curve of free DOX and TP5 (n = 3).

4.5. In vivo drug retention study

Since DOX possessed red fluorescent properties, an aqueous DOX solution was used as a control to assess drug release from TP5@DOX nanogels in mice. Mice were subcutaneously injected into the back with free DOX or TP5@DOX nanogel (10.0 mg•kg $^{-1}$ of DOX). Fluorescent images of mice were taken at prearranged time points to assess the drug retention of the TP5@DOX nanogel in mice.

4.6. In vitro cytotoxicity assessment

Melanoma cells were incubated with TP5, free DOX or TP5@DOX nanogels (quantitated by TP5: 4–64 μg•mL $^{-1}$, DOX: 0.5–8 μg•mL $^{-1}$) for 12 h and then replaced with DMEM 24 h later, the cytotoxicity of the TP5@DOX nanogel was evaluated through the MTT assay. Immunological cells were incubated with TP5, free DOX or TP5@DOX nanogels (quantitated by TP5: 2–16 μg•mL $^{-1}$, DOX: 0.25–2 μg•mL $^{-1}$) for 12 h and then evaluated the immune cytotoxicity of the TP5@DOX nanogel through the CCK8 assay. The viability of the cells was also assessed using double staining with Calcein-AM solution and then photographed by fluorescence microscopy.

4.7. Generation of intracellular ROS

Intracellular ROS production was assessed by DCFH-DA. In short, B16F10 cells were treated with 1.0 μM DCFH-DA and 10 μg•mL^{-1} Hoechst 33,342 for 40 min after treatment with TP5, free DOX or TP5@DOX nanogels (quantified as TP5: 16 μg mL^{-1}, DOX: 2 μg•mL^{-1}) for 12 h and then replaced with DMEM 24 h later [37]. After washing three times with DMEM, ROS production was analyzed qualitatively and quantitatively by fluorescence microscopy and flow cytometry, respectively.

4.8. Immunofluorescence assay

Cells were incubated on glass coverslips, differentially treated for 36 h, and then fixed in 4% paraformaldehyde. After washing with PBS, the cells were blocked with 5% FBS and then permeabilized with 0.3% Triton X-100. Cells were incubated using the specified primary antibody and Alexa Fluor secondary antibody. Images were observed with a confocal laser scanning microscope. (Carl Zeiss, Oberkochen, Germany).

4.9. In vitro co-culture experiment

B16F10 cells were treated with TP5, free DOX or TP5@DOX nanogels (quantified as TP5: 16 μg mL^{-1}, DOX: 2 μg mL^{-1}) for 12 h and then replaced with DMEM 24 h later, rather than directly treating the immunological cells. After that, the immunological cells were co-cultured with collected the supernatant for 48 h, followed by incubation with different antibodies for flow analysis [38,39].

4.10. ATP release assay

The extracellular ATP concentration was examined by ATP assay kits (Beyotime). ATP-induced chemiluminescence was measured by a Tecan Spark multimode microplate reader [40,41].

4.11. In vivo antitumor immune effect in the bilateral model

To evaluate the antitumor immune effect of the TP5@DOX nanogel, a bilateral tumor model was established. B16F10 cells (8.0×10^5) were subcutaneously injected into the right backs of 6 to 8-week-old C57BL/6 mice as the primary tumor, and the same number of B16F10 cells was injected into the other backs as the abscopal tumor after four days [42]. When the primary tumor volume was approximately 100 mm^3, the mice were randomly grouped into four groups of five mice each. Then the primary tumors received a single intratumoral injection of 100 μL PBS, TP5, free DOX, or TP5@DOX nanogel, respectively, with a dosage of 5.0 mg kg $^{-1}$ for free DOX and 40 mg kg $^{-1}$ for TP5. The body weight and tumor volumes were recorded every two days during the 2-week treatment. The tumor volume of mice was calculated based on the following equation.

$$\text{Tumor volume} = \frac{\text{L} \times W^2}{2}$$

where "L" and "W" refer to the largest and smallest diameter (mm) of tumors, respectively. After the 2-week treatment, the primary and abscopal tumors were collected separately. The inhibition ratio of primary and abscopal tumors was obtained based on the following equation.

$$\text{Tumor inhibition ratio}\% = \frac{(\text{W c} - \text{W t})}{\text{W c}} \times 100\%$$

where "Wc" and "Wt" represent the tumor weight (g) of the PBS group and the other groups, respectively.

To further monitor the tumor growth in mice, we established a bilateral tumor model in similar manner using luc-B16F10 cells for bioimaging experiments. We observed tumor growth at different time points (day 1, 5, 10) after injecting D-Luciferin, potassium salt. When the primary tumor volume reached about 100 mm^3, the mice were randomly divided into 4 groups (n = 5) and received a single intra-tumor injection with 100 μL PBS, TP5 (40.0 mg kg $^{-1}$), free DOX (5.0 mg kg $^{-1}$) or TP5@DOX nanogels (quantitated by TP5: 40 mg kg $^{-1}$, DOX: 5.0 mg kg $^{-1}$) in primary tumor, respectively.

4.11.1. Biosafety analyses

The removed liver, heart, spleen, lungs, and kidneys of the mice were removed were fixed in 4% paraformaldehyde for 48 h then examined for H&E. The collected orbital venous blood analyzed for ALT, AST, UR, CR and CK-MB levels [43,44].

4.12. TUNEL assay

Permeabilized tissue sections after different treatments. Fragmented DNA was labeled in situ using a Dead End Fluorometric TUNEL system (Promega). TUNEL-positive nuclei indicated apoptotic cells. Nucleus were stained with DAPI (Thermo Fisher Scientific) and photographed with fluorescence.

4.13. In vivo immune response study

The cell suspensions from lymph nodes were collected and stained with separate antibodies to quantify the proportion of matured DCs ($CD11c^+CD80^+CD86^+$) and regulatory cells (Treg cells, $CD4^+CD25^+FOXP3^+$). Additionally, the cell suspensions from primary tumors, abscopal tumors, and spleens were stained with antibodies separately to analyze the proportion of cytotoxic T cells (CTLs,

$CD3^+CD8^+$). T cells, DCs, and Treg cells were detected by flow cytometry.

4.14. In vivo metastasis inhibition efficiency evaluation

B16f10 cells were injected subcutaneously into the right backs of mice. When the tumor volume was approximately 50 mm3, B16F10 cells were reinjected into tumor-bearing mice by intravenous injection to establish a lung metastatic model. Mice were grouped and treated in the same manner as in previous studies. Lungs were collected after 3 weeks of treatment. Metastatic lesions in the lungs were recorded, and then the lungs were photographed and sectioned for H&E staining.

4.15. Statistical analysis

We used GraphPad Prism 8 software for statistical analysis (GraphPad Software, Inc., La Jolla, CA, USA). Differences among groups were conducted through ANOVA. Data between two groups were analyzed by independent Student's t-test. All data are presented as the mean with SD from at least three separate experiments. Significant differences between groups are indicated by $^*P < 0.05$, $^{**}P < 0.01$, and $^{***}P < 0.001$.

Authors' contributions

Ning Ding, Kai He and Hailong Tian: Project administration, Software, Data curation, Writing Original draft preparation. **Lei Li, Qiong Li, Shuaijun Lu, Ke Ding and Jiaqi Liu:** Methodology, Investigation, Formal analysis, Validation. **Edouard C. Nice:** Writing Original draft preparation, Writing-Review & Editing. **Wei Zhang:** Resources, Supervision, Funding acquisition. **Canhua Huang, Yong Tang and Zhisen Shen:** Conceptualization, Resources, Supervision, Project administration, Funding acquisition, Writing-Review & Editing.

Declaration of competing interest

The authors declare that they have no known competing financial interests or personal relationships that could have appeared to influence the work reported in this paper.

Data availability

Data will be made available on request.

Acknowledgments

This work was supported by Guangdong Basic and Applied Basic Research Foundation (No. 2019B030302012), National Key Research and Development Project (No. 2020YFA0509400), National Natural Science Foundation of China (No. 81821002 and 82130082), Ningbo Clinical Research Center for Otolaryngology Head and Neck Disease(No.2022L005), Ningbo Medical and Health Brand Discipline (No. PPXK2018-02), Ningbo "Technology Innovation 2025" Major Special Project (No. 2020Z097) and 1.3.5 project for disciplines of excellence, West China Hospital, Sichuan University (ZYJC21004 and ZYGD22007). The graphic scheme in this article was created with the BioRender platform. The authors appreciate the Pub-lab of West China School of Basic Medical Sciences & Forensic Medicine, Sichuan University, for providing several laboratory instruments. The authors also thank the Analytical & Testing Center of Sichuan University for providing several laboratory instruments.

Appendix A. Supplementary data

Supplementary data to this article can be found online at https://doi.org/10.1016/j.mtbio.2023.100645.

References

[1] S. Kakadia, N. Yarlagadda, R. Awad, M. Kundranda, J. Niu, B. Naraev, L. Mina, T. Dragovich, M. Gimbel, F. Mahmoud, Mechanisms of resistance to BRAF and MEK inhibitors and clinical update of US Food and Drug Administration-approved targeted therapy in advanced melanoma, OTT 11 (2018) 7095–7107, https://doi.org/10.2147/OTT.S182721.

[2] K. Saginala, A. Barsouk, J.S. Aluru, P. Rawla, A. Barsouk, Epidemiology of melanoma, Med. Sci. 9 (2021) 63, https://doi.org/10.3390/medsci9040063.

[3] L. Kuryk, L. Bertinato, M. Staniszewska, K. Pancer, M. Wieczorek, S. Salmaso, P. Caliceti, M. Garofalo, From conventional therapies to immunotherapy: melanoma treatment in review, Cancers 12 (2020) 3057, https://doi.org/10.3390/cancers12103057.

[4] S. Zhou, Q. Shang, N. Wang, Q. Li, A. Song, Y. Luan, Rational design of a minimalist nanoplatform to maximize immunotherapeutic efficacy: four birds with one stone, J. Contr. Release 328 (2020) 617–630, https://doi.org/10.1016/j.jconrel.2020.09.035.

[5] P. Zhang, J. Meng, Y. Li, C. Yang, Y. Hou, W. Tang, K.J. McHugh, L. Jing, Nanotechnology-enhanced immunotherapy for metastatic cancer, Innovation 2 (2021), 100174, https://doi.org/10.1016/j.xinn.2021.100174.

[6] T. Zhang, X. Qin, X. Cao, W. Li, T. Gong, Z. Zhang, Thymopentin-loaded phospholipid-based phase separation gel with long-lasting immunomodulatory effects: in vitro and in vivo studies, Acta Pharmacol. Sin. 40 (2019) 514–521, https://doi.org/10.1038/s41401-018-0085-8.

[7] S. Li, W. Zhang, R. Xing, C. Yuan, H. Xue, X. Yan, Supramolecular nanofibrils formed by coassembly of clinically approved drugs for tumor photothermal immunotherapy, Adv. Mater. 33 (2021), 2100595, https://doi.org/10.1002/adma.202100595.

[8] H.-Q. Wu, C.-C. Wang, Biodegradable smart nanogels: a new platform for targeting drug delivery and biomedical diagnostics, Langmuir 32 (2016) 6211–6225, https://doi.org/10.1021/acs.langmuir.6b00842.

[9] H. Tian, T. Zhang, S. Qin, Z. Huang, L. Zhou, J. Shi, E.C. Nice, N. Xie, C. Huang, Z. Shen, Enhancing the therapeutic efficacy of nanoparticles for cancer treatment using versatile targeted strategies, J. Hematol. Oncol. 15 (2022) 132, https://doi.org/10.1186/s13045-022-01320-5.

[10] Z. Li, L. Zhu, H. Sun, Y. Shen, D. Hu, W. Wu, Y. Wang, C. Qian, M. Sun, Fluorine assembly nanocluster breaks the shackles of immunosuppression to turn the cold tumor hot, Proc. Natl. Acad. Sci. U.S.A. 117 (2020) 32962–32969, https://doi.org/10.1073/pnas.2011297117.

[11] J. Fucikova, O. Kepp, L. Kasikova, G. Petroni, T. Yamazaki, P. Liu, L. Zhao, R. Spisek, G. Kroemer, L. Galluzzi, Detection of immunogenic cell death and its relevance for cancer therapy, Cell Death Dis. 11 (2020) 1013, https://doi.org/10.1038/s41419-020-03221-2.

[12] G. Kroemer, L. Galluzzi, O. Kepp, L. Zitvogel, Immunogenic cell death in cancer therapy, Annu. Rev. Immunol. 31 (2013) 51–72, https://doi.org/10.1146/annurev-immunol-032712-100008.

[13] H. Jin, C. Wan, Z. Zou, G. Zhao, L. Zhang, Y. Geng, T. Chen, A. Huang, F. Jiang, J.-P. Feng, J.F. Lovell, J. Chen, G. Wu, K. Yang, Tumor ablation and therapeutic immunity induction by an injectable peptide hydrogel, ACS Nano 12 (2018) 3295–3310, https://doi.org/10.1021/acsnano.7b08148.

[14] Q. Xue, H. Ren, C. Xu, G. Wang, C. Ren, J. Hao, D. Ding, Nanospheres of doxorubicin as cross-linkers for a supramolecular hydrogelation, Sci. Rep. 5 (2015) 8764, https://doi.org/10.1038/srep08764.

[15] X. Zhang, H. Zhou, Y. Xie, C. Ren, D. Ding, J. Long, Z. Yang, Rational design of multifunctional hetero-hexameric proteins for hydrogel formation and controlled delivery of bioactive molecules, Adv. Healthcare Mater. 3 (2014) 1804–1811, https://doi.org/10.1002/adhm.201300660.

[16] J. Dong, K. Wang, L. Sun, B. Sun, M. Yang, H. Chen, Y. Wang, J. Sun, L. Dong, Application of graphene quantum dots for simultaneous fluorescence imaging and tumor-targeted drug delivery, Sensor. Actuator. B Chem. 256 (2018) 616–623, https://doi.org/10.1016/j.snb.2017.09.200.

[17] B. Feng, F. Zhou, B. Hou, D. Wang, T. Wang, Y. Fu, Y. Ma, H. Yu, Y. Li, Binary cooperative prodrug nanoparticles improve immunotherapy by synergistically modulating immune tumor microenvironment, Adv. Mater. 30 (2018), 1803001, https://doi.org/10.1002/adma.201803001.

[18] C. Liang, X. Yan, R. Zhang, T. Xu, D. Zheng, Z. Tan, Y. Chen, Z. Gao, L. Wang, X. Li, Z. Yang, Enhanced cellular uptake and nuclear accumulation of drug-peptide nanomedicines prepared by enzyme-instructed self-assembly, J. Contr. Release 317 (2020) 109–117, https://doi.org/10.1016/j.jconrel.2019.11.028.

[19] B. Oresta, C. Pozzi, D. Braga, R. Hurle, M. Lazzeri, P. Colombo, N. Frego, M. Erreni, C. Faccani, G. Elefante, M. Barcella, G. Guazzoni, M. Rescigno, Mitochondrial metabolic reprogramming controls the induction of immunogenic cell death and efficacy of chemotherapy in bladder cancer, Sci. Transl. Med. 13 (2021), eaba6110, https://doi.org/10.1126/scitranslmed.aba6110.

[20] L. Galluzzi, I. Vitale, S. Warren, S. Adjemian, P. Agostinis, A.B. Martinez, T.A. Chan, G. Coukos, S. Demaria, E. Deutsch, D. Draganov, R.L. Edelson, S.C. Formenti, J. Fucikova, L. Gabriele, U.S. Gaipl, S.R. Gameiro, A.D. Garg, E. Golden, J. Han, K.J. Harrington, A. Hemminki, J.W. Hodge, D.M.S. Hossain, T. Illidge, M. Karin, H.L. Kaufman, O. Kepp, G. Kroemer, J.J. Lasarte, S. Loi, M.T. Lotze, G. Manic, T. Merghoub, A.A. Melcher, K.L. Mossman, F. Prosper, Ø. Rekdal, M. Rescigno, C. Riganti, A. Sistigu, M.J. Smyth, R. Spisek, J. Stagg, B.E. Strauss, D. Tang, K. Tatsuno, S.W. van Gool, P. Vandenabeele, T. Yamazaki, D. Zamarin, L. Zitvogel, A. Cesano, F.M. Marincola, Consensus guidelines for the definition, detection and interpretation of immunogenic cell death, J Immunother Cancer 8 (2020), e000337, https://doi.org/10.1136/jitc-2019-000337.

[21] C. Zhang, J. Song, L. Lou, X. Qi, L. Zhao, B. Fan, G. Sun, Z. Lv, Z. Fan, B. Jiao, J. Yang, Doxorubicin-loaded nanoparticle coated with endothelial cells-derived exosomes for immunogenic chemotherapy of glioblastoma, Bioeng. Transl. Med. 6 (2021), https://doi.org/10.1002/btm2.10203.
[22] H. Tian, L. Zhou, Y. Wang, E.C. Nice, C. Huang, H. Zhang, A targeted nanomodulator capable of manipulating tumor microenvironment against metastasis, J. Contr. Release 348 (2022) 590–600, https://doi.org/10.1016/j.jconrel.2022.06.022.
[23] K.S. Ravichandran, Beginnings of a good apoptotic meal: the find-me and eat-me signaling pathways, Immunity 35 (2011) 445–455, https://doi.org/10.1016/j.immuni.2011.09.004.
[24] X. Ren, N. Wang, Y. Zhou, A. Song, G. Jin, Z. Li, Y. Luan, An injectable hydrogel using an immunomodulating gelator for amplified tumor immunotherapy by blocking the arginase pathway, Acta Biomater. 124 (2021) 179–190, https://doi.org/10.1016/j.actbio.2021.01.041.
[25] Q. Li, Z. Zhao, X. Qin, M. Zhang, Q. Du, Z. Li, Y. Luan, A checkpoint-regulatable immune niche created by injectable hydrogel for tumor therapy, Adv. Funct. Mater. 31 (2021), 2104630, https://doi.org/10.1002/adfm.202104630.
[26] R. Strauss, A. Cressman, M. Cheung, A. Weinerman, S. Waldman, E. Etchells, A. Zahirieh, P. Tartaro, J. Rezmovitz, J. Callum, Major reductions in unnecessary aspartate aminotransferase and blood urea nitrogen tests with a quality improvement initiative, BMJ Qual. Saf. 28 (2019) 809–816, https://doi.org/10.1136/bmjqs-2018-008991.
[27] H. Huang, Z. Shen, Q. Geng, Z. Wu, P. Shi, X. Miao, Protective effect of Schisandra chinensis bee pollen extract on liver and kidney injury induced by cisplatin in rats, Biomed. Pharmacother. 95 (2017) 1765–1776, https://doi.org/10.1016/j.biopha.2017.09.083.
[28] S. Alpsoy, C. Aktas, R. Uygur, B. Topcu, M. Kanter, M. Erboga, O. Karakaya, A. Gedikbasi, Antioxidant and anti-apoptotic effects of onion (*Allium cepa*) extract on doxorubicin-induced cardiotoxicity in rats: antioxidant and anti-apoptotic effects of ACE on cardiotoxicity, J. Appl. Toxicol. 33 (2013) 202–208, https://doi.org/10.1002/jat.1738.
[29] J. Zhou, G. Wang, Y. Chen, H. Wang, Y. Hua, Z. Cai, Immunogenic cell death in cancer therapy: present and emerging inducers, J. Cell Mol. Med. 23 (2019) 4854–4865, https://doi.org/10.1111/jcmm.14356.
[30] M. Shahverdi, J. Masoumi, F. Ghorbaninezhad, N. Shajari, F. Hajizadeh, H. Hassanian, N. Alizadeh, M. Jafarlou, B. Baradaran, The modulatory role of dendritic cell-T cell cross-talk in breast cancer: challenges and prospects, Adv. Med. Sci. 67 (2022) 353–363, https://doi.org/10.1016/j.advms.2022.09.001.
[31] F. Broere, W. van Eden, T cell subsets and T cell-mediated immunity, in: M.J. Parnham, F.P. Nijkamp, A.G. Rossi (Eds.), Nijkamp and Parnham's Principles of Immunopharmacology, Springer International Publishing, Cham, 2019, pp. 23–35, https://doi.org/10.1007/978-3-030-10811-3_3.
[32] O.A.W. Haabeth, M. Fauskanger, M. Manzke, K.U. Lundin, A. Corthay, B. Bogen, A.A. Tveita, CD4+ T-cell–mediated rejection of MHC class II–positive tumor cells is dependent on antigen secretion and indirect presentation on host APCs, Cancer Res. 78 (2018) 4573–4585, https://doi.org/10.1158/0008-5472.CAN-17-2426.
[33] R. Kennedy, E. Celis, Multiple roles for CD4 $^{+}$ T cells in anti-tumor immune responses, Immunol. Rev. 222 (2008) 129–144, https://doi.org/10.1111/j.1600-065X.2008.00616.x.
[34] H. Nishikawa, T. Kato, I. Tawara, K. Saito, H. Ikeda, K. Kuribayashi, P.M. Allen, R.D. Schreiber, S. Sakaguchi, L.J. Old, H. Shiku, Definition of target antigens for naturally occurring CD4+ CD25+ regulatory T cells, J. Exp. Med. 201 (2005) 681–686, https://doi.org/10.1084/jem.20041959.
[35] W. Zou, Regulatory T cells, tumour immunity and immunotherapy, Nat. Rev. Immunol. 6 (2006) 295–307, https://doi.org/10.1038/nri1806.
[36] Y. Zhou, T. Ye, C. Ye, C. Wan, S. Yuan, Y. Liu, T. Li, F. Jiang, J.F. Lovell, H. Jin, J. Chen, Secretions from hypochlorous acid-treated tumor cells delivered in a melittin hydrogel potentiate cancer immunotherapy, Bioact. Mater. 9 (2022) 541–553, https://doi.org/10.1016/j.bioactmat.2021.07.019.
[37] S. Lu, H. Tian, L. Li, B. Li, M. Yang, L. Zhou, H. Jiang, Q. Li, W. Wang, E.C. Nice, N. Xie, C. Huang, L. Liu, Nanoengineering a zeolitic imidazolate framework-8 capable of manipulating energy metabolism against cancer chemo-phototherapy resistance, Small 18 (2022), 2204926, https://doi.org/10.1002/smll.202204926.
[38] S. Tokhanbigli, H. Alavifard, H. Asadzadeh Aghdaei, M.R. Zali, K. Baghaei, Combination of pioglitazone and dendritic cell to optimize efficacy of immune cell therapy in CT26 tumor models, Bioimpacts (2022) 1, https://doi.org/10.34172/bi.2022.24209.
[39] S. Moise, L. Dolcetti, F. Dazzi, P. Roach, L. Buttery, S. MacNeil, N. Medcalf, Assessing the immunosuppressive activity of alginate-encapsulated mesenchymal stromal cells on splenocytes, Artificial Cells, Nanomed. Biotechnol. 50 (2022) 168–176, https://doi.org/10.1080/21691401.2022.2088547.
[40] L. Li, H. Tian, Z. Zhang, N. Ding, K. He, S. Lu, R. Liu, P. Wu, Y. Wang, B. He, M. Luo, P. Peng, M. Yang, E.C. Nice, C. Huang, N. Xie, D. Wang, W. Gao, Carrier-free nanoplatform via evoking pyroptosis and immune response against breast cancer, ACS Appl. Mater. Interfaces 15 (2023) 452–468, https://doi.org/10.1021/acsami.2c17579.
[41] P. Jin, J. Jiang, L. Zhou, Z. Huang, S. Qin, H. Chen, L. Peng, Z. Zhang, B. Li, M. Luo, T. Zhang, H. Ming, N. Ding, L. Li, N. Xie, W. Gao, W. Zhang, E.C. Nice, Y. Wei, C. Huang, Disrupting metformin adaptation of liver cancer cells by targeting the TOMM34/ATP5B axis, EMBO Mol. Med. 14 (2022), https://doi.org/10.15252/emmm.202216082.
[42] H. Ming, B. Li, H. Tian, L. Zhou, J. Jiang, T. Zhang, L. Qiao, P. Wu, E.C. Nice, W. Zhang, W. He, C. Huang, H. Zhang, A minimalist and robust chemo-photothermal nanoplatform capable of augmenting autophagy-modulated immune response against breast cancer, Materials Today Bio 15 (2022), 100289, https://doi.org/10.1016/j.mtbio.2022.100289.
[43] H. Tian, J. Cao, B. Li, Edouard C. Nice, H. Mao, Y. Zhang, C. Huang, Managing the immune microenvironment of osteosarcoma: the horizons for osteosarcoma treatment, Bone Res. 11 (2023) 11, https://doi.org/10.1038/s41413-023-00246-z.
[44] W. Jia, H. Tian, J. Jiang, L. Zhou, L. Li, M. Luo, N. Ding, E.C. Nice, C. Huang, H. Zhang, Brain-Targeted HFn-Cu-REGO nanoplatform for site-specific delivery and manipulation of autophagy and cuproptosis in glioblastoma, Small 19 (2023), 2205354, https://doi.org/10.1002/smll.202205354.